

Coexistence of extended flat band and Kekulé order in Li-intercalated graphene

Changhua Bao,^{1,*} Hongyun Zhang,^{1,*} Xi Wu,² Shaohua Zhou,¹ Qian Li,¹ Pu Yu,^{1,3} Jia Li,² Wenhui Duan,^{1,3} and Shuyun Zhou^{1,3,†}

¹*State Key Laboratory of Low-Dimensional Quantum Physics and Department of Physics, Tsinghua University, Beijing 100084, P. R. China*

²*Shenzhen Geim Graphene Center and Institute of Materials Research, Tsinghua Shenzhen International Graduate School, Tsinghua University, Shenzhen 518055, P. R. China*

³*Frontier Science Center for Quantum Information, Beijing 100084, P. R. China*

(Dated: April 29, 2022)

Doping graphene near the 1/4 filling to shift the extended flat band and van Hove singularity below E_F has been highly desirable. Here we report the experimental observation of an extended flat band below E_F in Li-intercalated graphene. Strong electron-phonon interaction is clearly identified by notable kinks in the band dispersion. Moreover, the evolution of the band structure upon Li intercalation shows that the extended flat band and the Kekulé order emerge simultaneously. Our work provides opportunities for investigating flat band related instabilities and its interplay with the Kekulé order.

In solids, a flat band with a high density of states (DOS) near the Fermi energy E_F can enhance many-body interactions such as electron-phonon (el-ph) interaction and electron-electron correlation, thereby increasing instabilities toward exotic ordered states. For example, in magic-angle twisted bilayer graphene (MABLG) [1], the flat band can be induced through hybridization of the Dirac cones via the moiré superlattice potential and novel phenomena such as superconductivity [2], Mott insulator [3] and charge order [4] have been discovered. Instead of band hybridization near the Dirac point, a different strategy for inducing a flat band is doping graphene to near 1/4 filling, so that the extended flat band near the van Hove singularity (VHS, see Fig. 1(a) for schematic band structure) is shifted to E_F . Graphene near 1/4 filling has attracted extensive interests with intriguing predictions such as instabilities toward d -wave superconductivity by repulsive electron-electron interaction [5–7], topological superconductivity [8], and chiral spin density wave [9, 10].

In graphene, the π^* band VHS is at ~ 3 eV above the Dirac point, and an extremely high electron doping is required to shift it to E_F . Experimentally, electron doping of graphene has been achieved by adsorption of alkaline metals [11–16] or Gd, Yb [17–20]. In particular, combining Yb intercalation with K adsorption dopes graphene beyond the VHS [20], however, the Dirac cone of graphene is severely distorted due to the hybridization with the 4f orbital of Yb. In this work, we report the existence of an extended flat band near 1/4 doping in Li-intercalated graphene by angle-resolved photoemission spectroscopy (ARPES) measurements. Significant band renormalization is observed as a result of strong el-ph interaction. Moreover, by monitoring the evolution of the extended flat band and replica Dirac cone upon Li intercalation, we find that the extended flat band and

the Kekulé order co-develop, suggesting a strong connection between these two intriguing properties and providing important insights for understanding the underlying mechanism.

The Li-intercalated bilayer graphene is obtained by intercalating Li [21, 22] to monolayer graphene on SiC substrate [23] (see Methods in [24]). Figure 1(b) shows an overview of the three-dimensional electronic structure from ARPES measurements. The replica pockets around the Γ point indicate the Kekulé order and chiral symmetry breaking reported recently [22]. In this work, we focus on a different aspect, namely, the existence of extended flat band with strong el-ph interaction near 1/4 doping and its connection to the Kekulé order. Two large pockets labeled as α and β are observed near each Brillouin zone (BZ) corner with the Dirac points at energies of -1.27 and -1.82 eV, indicating a higher doping level than previously reported Li-intercalated graphene [13, 15, 21, 25]. The Dirac point energy of -1.82 eV is at even lower energy than the -1.6 eV in Yb-intercalated graphene [20]. The absence of hybridization is in overall agreement with calculated electronic structure [26] and distinguishes it from Ca-intercalated graphene [13, 14, 26] or Yb-intercalated graphene [20]. Such high electron doping is made possible by monitoring the electronic structure with ARPES measurements in real time during Li intercalation, which allows to achieve the optimum doping level (see Fig. S1-3 and attached movie for more details in [24]).

Figure 2(a) shows the Fermi surface map, from which the carrier concentrations can be directly extracted from the size of the Fermi pockets through the Luttinger theorem [27]. The extracted carrier concentrations are $1.3 \times 10^{14} \text{ cm}^{-2}$ and $4.3 \times 10^{14} \text{ cm}^{-2}$ for α and β pockets respectively, which are equivalent to 0.07 and 0.23 electrons per unit cell. Even higher carrier concentrations of

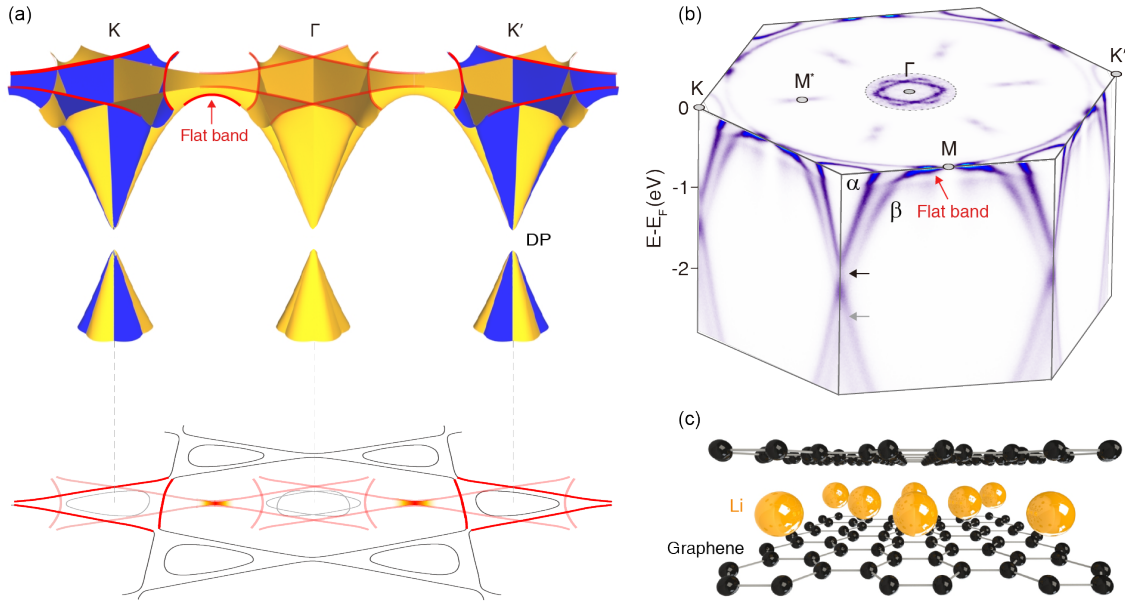


FIG. 1: (a) A schematic for the flat band near the van Hove singularity point in Kekulé-ordered graphene and constant energy maps of the Dirac cones. (b) The full three-dimensional electronic structure of Kekulé-ordered graphene measured by ARPES. The intensity inside the dashed circle around Γ is enhanced by a multiplication factor of 15 for better visualization. (c) A schematic drawing of Li-intercalated bilayer graphene.

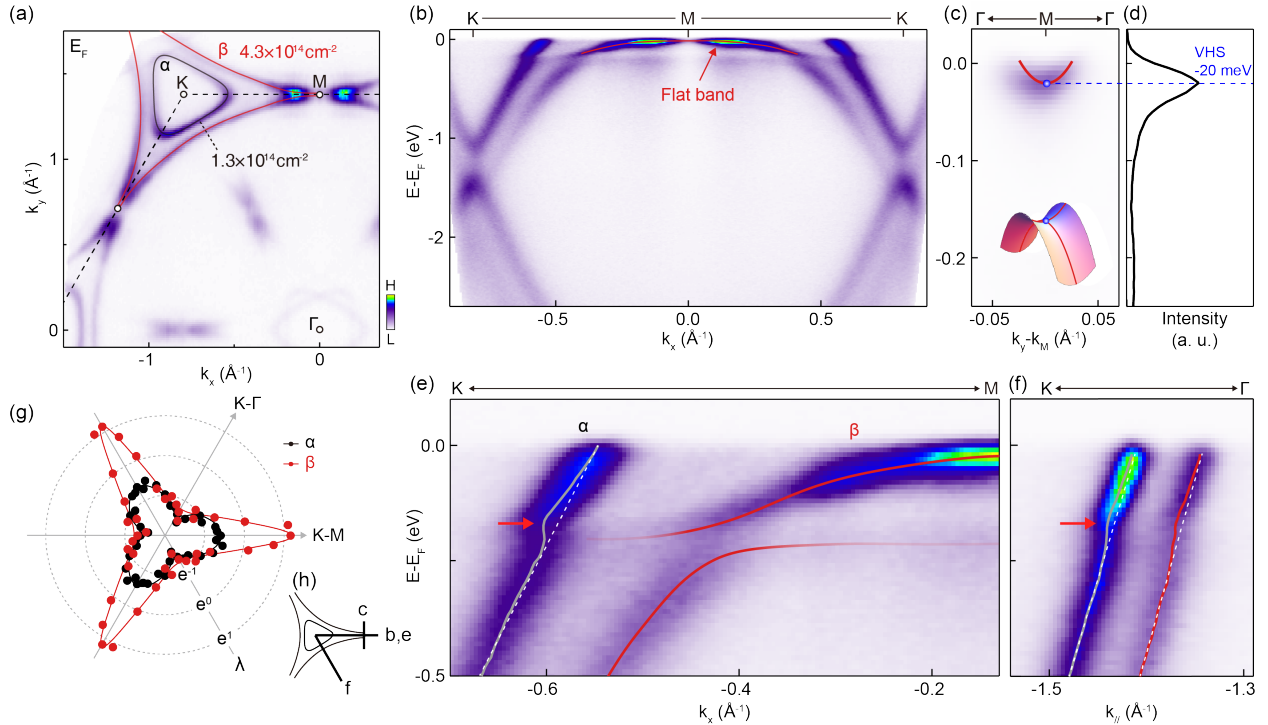


FIG. 2: (a) Fermi surface map. (b) Dispersion image along the K-M-K direction. (c) Dispersion image along the Γ -M- Γ direction. The inset is a schematic of the saddle point. (d) EDC at the M point, showing that the VHS (blue dot) is at -20 meV . (e) Dispersion image around E_F along the K-M direction. (f) Dispersion image around E_F along the K- Γ direction. (g) Extracted angular dependence of el-ph coupling constant of two bands. (h) Schematics for directions of corresponding dispersion images.

$1.4 \times 10^{14} \text{ cm}^{-2}$ and $5.1 \times 10^{14} \text{ cm}^{-2}$, which correspond to 0.08 and 0.27 electrons per unit cell, can be obtained by second Li intercalation of the same sample after annealing (see Methods and Fig. S4 in [24]). The high carrier concentration is in line with the superdense Li intercalation between two graphene sheets with estimated carrier concentration of $4 \times 10^{14} \text{ cm}^{-2}$ [28], and here we can resolve each electron pocket and extract the corresponding carrier concentration directly.

Figure 2(b) and 2(c) shows dispersion images measured along two high symmetry directions through the M point. The dispersion is quite flat when approaching the M point and extended in a large momentum range. This corresponds to the top of the valence band along the K-M direction (Fig. 2(b)) and the bottom of the conduction band along the Γ -M direction (Fig. 2(c)), indicating that it is a saddle point (schematic in the inset of Fig. 2(c)). Energy distribution curve (EDC) at the M point shows that the saddle point VHS is at -20 meV, thus Li-intercalated graphene provides an important platform for investigating flat band induced instabilities around the $1/4$ filling [8–10]. Importantly, the doping beyond the VHS and the absence of hybridization or orbital contribution from the intercalated Li, allow to probe the many-body interactions of the intrinsic Dirac fermions.

The high carrier concentration leads to strong el-ph coupling. Figure 2(e) shows a zoom-in of the dispersion image near E_F . For the α pocket which does not reach the doping level of the VHS, a renormalization of the dispersion, a kink, is clearly observed at the energy of $-180 \pm 20 \text{ meV}$ (pointed by the red arrow), while for the β band which is beyond the VHS, the el-ph coupling is even stronger, with a strongly deviated dispersion at similar energy. Comparison of this phonon energy with the calculated phonon dispersion for the Kekulé-ordered graphene [29] shows that the phonons that are coupled with electrons are the in-plane optical phonon A_{1g} . The extracted el-ph coupling strength from the renormalization of the Fermi velocity (see Fig. S5 for more details in [24]) is $\lambda_{\alpha}^{KM} = 0.55$ along the K-M direction for the α pocket, and $\lambda_{\beta}^{KM} = 3.19$ for the β pocket. The el-ph coupling constant is quite anisotropic, and the el-ph coupling strength is reduced to $\lambda_{\alpha}^{K\Gamma} = 0.25$ and $\lambda_{\beta}^{K\Gamma} = 0.27$ along the K- Γ direction (Fig. 2(f)). The anisotropic ratio increases from 2.2 for the α pocket (black symbols in Fig. 2(g)) to 11.8 for the β pocket (red symbols in Fig. 2(g)). The el-ph coupling constant is larger than previously reported values of $\lambda = 0.14$ to 0.61 for pristine graphene [30], alkaline metal doped graphene [31, 32], superconducting Li or Ca doped graphene [26, 33] and graphite [34], due to the higher carrier concentration here. Such strong el-ph coupling may favor instabilities such as superconductivity in graphene and graphite [34–36]. For example, superconductivity with T_c of up to 8.1 K has been predicated in monolayer LiC_6 due

to the enhanced el-ph coupling [26]. Experimentally, the superconducting gap has been reported in Li-doped graphene [33] and the Meissner effect has been reported in Li-intercalated graphene [37]. Here, the observation of stronger el-ph coupling in Li-intercalated graphene provides new possibilities for achieving superconductivity with a higher T_c , and future experimental efforts such as transport measurements are needed.

To further investigate if there is any correlation between the extended flat band and Kekulé order, we show in Fig. 3 the evolution of the electronic structures during the Li intercalation process. Here the size of the Fermi pocket (Fig. 3(a)-(f)) is used to quantify the carrier concentration, while the dispersions near K (middle panels) and near Γ (Fig. 3(g)-(l)) are used to monitor the extended flat band and the Kekulé order respectively. Upon Li deposition, the carrier concentration increases, and at carrier concentration of $n = 0.9 \times 10^{14} \text{ cm}^{-2}$ (see Fig. 3(c)), a new Dirac cone appears, indicating decoupling of the buffer layer from the SiC substrate and the formation of two graphene layers [25]. More Li deposition leads to increasing electron doping, and the replica Dirac cone at the Γ point becomes detectable at a carrier concentration of $n = 3.2 \times 10^{14} \text{ cm}^{-2}$ (Fig. 3(j)), indicating the formation of the Kekulé order. Further Li deposition leads to a larger β pocket (Fig. 3(e)), and the flat band intensity becomes stronger and finally saturated at $n = 5.6 \times 10^{14} \text{ cm}^{-2}$ (Fig. 3(f)). The emergence of both the extended flat band and replica Dirac cones near Γ suggests that they not only coexist, but also are strongly connected.

To further confirm the co-development of the extended flat band and the Kekulé order, Figure 4(a) shows the continuous evolution of the electronic structure during Li intercalation, and a quantitative analysis of the intensity for the extended flat band and the replica Dirac cone is shown in Fig. 4(c). A comparison of the temporal evolution of the intensity for the extended flat band (red triangle in Fig. 4(c)) and replica Dirac cone (blue circle) shows that they have the same trend, and they both increase with the carrier concentration of the β pocket (red symbol in Fig. 4(b)), thereby confirming the coexistence and co-development of the flat band and the Kekulé order.

To understand the coexistence of the Kekulé order and the extended flat band, we first discuss the possible mechanisms of the Kekulé order. There are three main types of mechanisms for the Kekulé order: Friedel oscillation mediated adatom interaction, screened Coulomb interaction between adatoms, and adatom-substrate interaction. The Friedel oscillation mediated adatom interaction is the most well-known mechanism for realizing hidden Kekulé order in graphene with dilute adatoms [38, 39], where the adatoms interact with each other coherently through the Friedel oscillation, and the charge density oscillates with a wavelength $\lambda = \pi/k_F$ (k_F is the

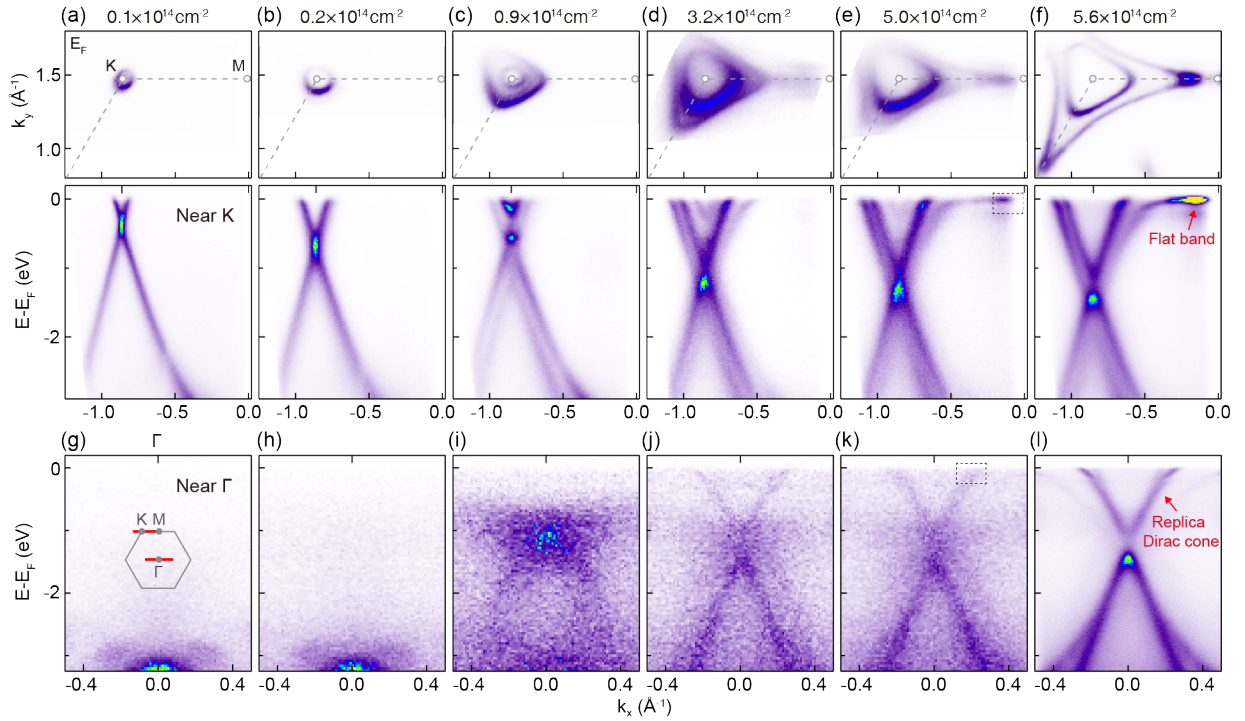


FIG. 3: (a-f) Fermi surface maps around the K point and dispersion images along the K-M direction at different doping levels (total carrier concentration). (g-l) Dispersion images along the Γ -K direction at different doping levels the same as (a-f). The inset in (g) indicates the directions of dispersion images in (a-f) and (g-l).

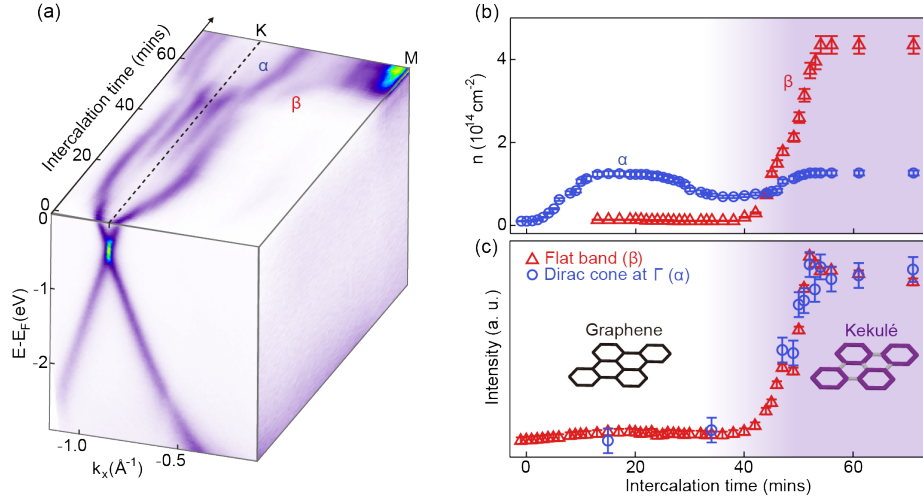


FIG. 4: (a) Continuous evolution of the band structures during Li intercalation. (b) Evolution of carrier concentration for two bands α and β during Li intercalation. (c) Intensity evolution of flat band and replica Dirac cone during Li intercalation, by integrating the ARPES intensity inside the black dashed boxes in the bottom panel of Fig. 3(e) and Fig. 3(k) respectively. The error bars are estimated from the noise level.

Fermi wave vector) to form ordered states. For pristine graphene, k_F is equal to Γ -K distance and λ is equal to the period of Kekulé order, thereby favoring the formation of the Kekulé order. However, this picture becomes invalid at high doping, because k_F strongly deviates from Γ -K distance and λ is no longer equal to the period of

the Kekulé order, making it an unlikely mechanism for our Li-intercalated graphene.

The more likely mechanism for the Kekulé order is the direct Coulomb repulsion, complemented by adatom-substrate interaction. The Coulomb repulsion interaction would be screened by graphene, leading to the smaller ef-

fective charge and faster decay, however, since the intercalated Li atoms are highly ionized, a stronger Coulomb interaction is expected, increasing the possibility of forming ordered states [40]. This, however, is not sufficient to determine the Kekulé order, and adatom-substrate interaction needs to be taken into account, in order to enforce the adatoms to stay in specific positions to maintain the lowest energy, namely the templating effect [41, 42]. Our first-principles calculations show the hollow site of graphene has the lowest energy (-1.06 eV) for a Li atom than the top (-0.87 eV) or bridge (-0.93 eV) site [22], and therefore Li atoms prefer the hollow sites and modify the C-C bonding surrounding them, leading to Kekulé-O type bond texture. Therefore, the screened Coulomb interaction and adatom-substrate interaction jointly lead to the formation of the Kekulé order in the Li-intercalated graphene.

Along this line, the co-development of the extended flat band and the Kekulé order can now be understood as the following. The emergence of the flat band relies on the large charge transfer from Li, while the residual positive charge in the Li ions enhances the screened Coulomb repulsion interaction, thus favoring the formation of Kekulé order. In this way, the extended flat band and the Kekulé order are intrinsically linked by the charge transfer which contributes to the large doping and the induced Coulomb interaction. This picture is also supported by first-principles calculations (see Fig. S6 for more details in [24]).

In summary, we report the coexistence of the extended flat band and the Kekulé order in Li-intercalated graphene, thereby identifying an intriguing platform for investigating both electronic instabilities [5–10] and Kekulé order related physics [43, 44]. Whether the flat band and the Kekulé order can interact with each other is an interesting open question which needs more investigations in the future, in particular, their interplay may lead to new complex ordered phases by coupling the nesting vector [9, 10] and the Kekulé order vector, and intriguing Kekulé superconductivity [45].

ACKNOWLEDGMENTS

We thank Hong Yao, Congjun Wu and Peizhe Tang for useful discussions. This work was supported by the National Key R&D Program of China (Grants No. 2021YFA1400100, 2020YFA0308800), the National Natural Science Foundation of China (Grant No. 11725418). J. L. was supported by the National Natural Science Foundation of China (Grant No. 11874036) and Local Innovative and Research Teams Project of Guangdong Pearl River Talents Program (2017BT01N111).

- * These authors contributed equally to this work.
 † Correspondence should be sent to syzhou@mail.tsinghua.edu.cn
- [1] R. Bistritzer and A. H. MacDonald, Proc. Natl. Acad. Sci. U.S.A. **108**, 12233 (2011).
 - [2] Y. Cao, V. Fatemi, S. Fang, K. Watanabe, T. Taniguchi, E. Kaxiras, and P. Jarillo-Herrero, Nature **556**, 43 (2018).
 - [3] Y. Cao, V. Fatemi, A. Demir, S. Fang, S. L. Tomarken, J. Y. Luo, J. D. Sanchez-Yamagishi, K. Watanabe, T. Taniguchi, E. Kaxiras, et al., Nature **556**, 80 (2018).
 - [4] Y. Jiang, X. Lai, K. Watanabe, T. Taniguchi, K. Haule, J. Mao, and E. Y. Andrei, Nature **573**, 91 (2019).
 - [5] A. M. Black-Schaffer and S. Doniach, Phys. Rev. B **75**, 134512 (2007).
 - [6] S. Raghu, S. A. Kivelson, and D. J. Scalapino, Phys. Rev. B **81**, 224505 (2010).
 - [7] S. Pathak, V. B. Shenoy, and G. Baskaran, Phys. Rev. B **81**, 085431 (2010).
 - [8] R. Nandkishore, L. S. Levitov, and A. V. Chubukov, Nat. Phys. **8**, 158 (2012).
 - [9] W.-S. Wang, Y.-Y. Xiang, Q.-H. Wang, F. Wang, F. Yang, and D.-H. Lee, Phys. Rev. B **85**, 035414 (2012).
 - [10] S. Jiang, A. Meszaros, and Y. Ran, Phys. Rev. X **4**, 031040 (2014).
 - [11] J. L. McChesney, A. Bostwick, T. Ohta, T. Seyller, K. Horn, J. González, and E. Rotenberg, Phys. Rev. Lett. **104**, 136803 (2010).
 - [12] K. Sugawara, K. Kanetani, T. Sato, and T. Takahashi, AIP Adv. **1**, 022103 (2011).
 - [13] K. Kanetani, K. Sugawara, T. Sato, R. Shimizu, K. Iwaya, T. Hitosugi, and T. Takahashi, Proc. Natl. Acad. Sci. U.S.A. **109**, 19610 (2012).
 - [14] R. Shimizu, K. Sugawara, K. Kanetani, K. Iwaya, T. Sato, T. Takahashi, and T. Hitosugi, Phys. Rev. Lett. **114**, 146103 (2015).
 - [15] N. M. Caffrey, L. I. Johansson, C. Xia, R. Armiento, I. A. Abrikosov, and C. Jacobi, Phys. Rev. B **93**, 195421 (2016).
 - [16] M. G. Hell, N. Ehlen, B. V. Senkovskiy, E. H. Hasdeo, A. Fedorov, D. Dombrowski, C. Busse, T. Michely, G. di Santo, L. Petaccia, et al., Nano Lett. **18**, 6045 (2018).
 - [17] S. Link, S. Forti, A. Stöhr, K. Küster, M. Rösner, D. Hirschmeier, C. Chen, J. Avila, M. C. Asensio, A. A. Zakharov, et al., Phys. Rev. B **100**, 121407(R) (2019).
 - [18] C. Hwang, D. Y. Kim, D. A. Siegel, K. T. Chan, J. Noffsinger, A. V. Fedorov, M. L. Cohen, B. Johansson, J. B. Neaton, and A. Lanzara, Phys. Rev. B **90**, 115417 (2014).
 - [19] P. Rosenzweig, H. Karakachian, S. Link, K. Küster, and U. Starke, Phys. Rev. B **100**, 035445 (2019).
 - [20] P. Rosenzweig, H. Karakachian, D. Marchenko, K. Küster, and U. Starke, Phys. Rev. Lett. **125**, 176403 (2020).
 - [21] C. Virojanadara, S. Watcharinyanon, A. A. Zakharov, and L. I. Johansson, Phys. Rev. B **82**, 205402 (2010).
 - [22] C. Bao, H. Zhang, T. Zhang, X. Wu, L. Luo, S. Zhou, Q. Li, Y. Hou, W. Yao, L. Liu, et al., Phys. Rev. Lett. **126**, 206804 (2021).
 - [23] Q. Wang, W. Zhang, L. Wang, K. He, X. Ma, Q. Xue, Large-scale uniform bilayer graphene prepared by vac-

- uum graphitization of 6H-SiC(0001) substrates. *J. Phys. Condens. Matter.* **25**, 095002 (2013).
- [24] See the Supplemental Material for additional information about the materials and methods.
- [25] F. Bisti, G. Profeta, H. Vita, M. Donarelli, F. Perrozzi, P. M. Sheverdyaeva, P. Moras, K. Horn, and L. Ottaviano, *Phys. Rev. B* **91**, 245411 (2015).
- [26] G. Profeta, M. Calandra, and F. Mauri, *Nat. Phys.* **8**, 131 (2012).
- [27] J. M. Luttinger, *Phys. Rev.* **119**, 1153 (1960).
- [28] M. Kühne, F. Börrnert, S. Fecher, M. Ghorbani-Asl, J. Biskupek, D. Samuelis, A. V. Krasheninnikov, U. Kaiser, and J. H. Smet, *Nature* **564**, 234 (2018).
- [29] H. Zhang, C. Bao, M. Schuler, S. Zhou, Q. Li, L. Luo, W. Yao, Z. Wang, T. P. Devereaux, and S. Zhou, *Natl. Sci. Rev.* nwab175 (2021).
- [30] S. Y. Zhou, D. A. Siegel, A. V. Fedorov, and A. Lanzara, *Phys. Rev. B* **78**, 193404 (2008).
- [31] A. Bostwick, T. Ohta, T. Seyller, K. Horn, and E. Rotenberg, *Nat. Phys.* **3**, 36 (2007).
- [32] A. V. Fedorov, N. I. Verbitskiy, D. Haberer, C. Struzzi, L. Petaccia, D. Usachov, O. Y. Vilkov, D. V. Vyalikh, J. Fink, M. Knupfer, et al., *Nat. Commun.* **5**, 3257 (2014).
- [33] B. M. Ludbrook, G. Levy, P. Nigge, M. Zonno, M. Schneider, D. J. Dvorak, C. N. Veenstra, S. Zhdanovich, D. Wong, P. Dosanjh, et al., *Proc. Natl. Acad. Sci. U.S.A.* **112**, 11795 (2015).
- [34] T. Valla, J. Camacho, Z.-H. Pan, A. V. Fedorov, A. C. Walters, C. A. Howard, and M. Ellerby, *Phys. Rev. Lett.* **102**, 107007 (2009).
- [35] Z. H. Pan, J. Camacho, M. H. Upton, A. V. Fedorov, C. A. Howard, M. Ellerby, and T. Valla, *Phys. Rev. Lett.* **106**, 187002 (2011).
- [36] S. L. Yang, J. A. Sobota, C. A. Howard, C. J. Pickard, M. Hashimoto, D. H. Lu, S. K. Mo, P. S. Kirchmann, and Z. X. Shen, *Nat. Commun.* **5**, 3493 (2014).
- [37] A. P. Tiwari, S. Shin, E. Hwang, S. G. Jung, T. Park, and H. Lee, *J. Phys. Condens. Matter* **29**, 445701 (2017).
- [38] V. V. Cheianov, V. I. Fal'ko, O. Syljuasen, and B. L. Altshuler, *Solid State Commun.* **149**, 1499 (2009).
- [39] C. Gutiérrez, C.-J. Kim, L. Brown, T. Schiros, D. Nordlund, E. B. Lochochok, K. Shen, J. Park, and A. Pasupathy, *Nat. Phys.* **12**, 950 (2016).
- [40] C.-L. Song, B. Sun, Y.-L. Wang, Y.-P. Jiang, L. Wang, K. He, X. Chen, P. Zhang, X.-C. Ma, and Q.-K. Xue, *Phys. Rev. Lett.* **108**, 156803 (2012).
- [41] J.-L. Li, J.-F. Jia, X.-J. Liang, X. Liu, J.-Z. Wang, Q.-K. Xue, Z.-Q. Li, J. S. Tse, Z. Zhang, and S. B. Zhang, *Phys. Rev. Lett.* **88**, 066101 (2002).
- [42] D. Ma, Z. Fu, X. Sui, K. Bai, J. Qiao, C. Yan, Y. Zhang, J. Hu, Q. Xiao, X. Mao, et al., *ACS Nano* **12**, 10984 (2018).
- [43] C.-Y. Hou, C. Chamon, and C. Mudry, *Phys. Rev. Lett.* **98**, 186809 (2007).
- [44] E. Andrade, R. Carrillo-Bastos, and G. G. Naumis, *Phys. Rev. B* **99**, 035411 (2019).
- [45] B. Roy and I. F. Herbut, *Phys. Rev. B* **82**, 035429 (2010).